Appl Nanosci (2016) 6:503–510
DOI 10.1007/s13204-015-0448-0

ORIGINAL ARTICLE

Synthesis, optical, photocatalytic, and electrochemical studies on Ag_2S/ZnS and ZnS/Ag_2S nanocomposites

G. Murugadoss[1] · R. Jayavel[1] · M. Rajesh Kumar[2] · R. Thangamuthu[3]

Received: 3 February 2015 / Accepted: 10 April 2015 / Published online: 3 June 2015

Abstract Novel Ag_2S/ZnS and ZnS/Ag_2S nanocomposites were synthesized by a simple chemical method in air. Different morphologies were obtained for Ag_2S/ZnS nanocomposites annealed at different temperatures. The products were characterized by X-ray diffraction (XRD), scanning electron microscopy (SEM), UV–visible absorption, and photoluminescence (PL) spectroscopy. Thermal stability and phase transition of the sample were studied by TG–DTA. Compared the PL spectra of Ag_2S/ZnS at 640 nm, it was significantly red shifted from 640 to 670 nm for reversed ZnS/Ag_2S nanocomposites. The band gaps of nanocomposites were lying between 2.25 and 2.55 eV range. It has been found that as-synthesized powder has excellent photocatalytic activity toward degradation of methylene blue (MB) under visible light and electrochemical activity, indicating that Ag_2S/ZnS and ZnS/Ag_2S nanocomposites can play an important role as semiconductor photocatalyst and energy storage applications.

✉ G. Murugadoss
murugadoss_g@yahoo.com

[1] Centre for Nanoscience and Technology, Anna University, Chennai 600025, Tamilnadu, India

[2] Department of Physics, Annamalai University, Annamalai Nagar 608002, Tamilnadu, India

[3] Electrochemical Materials Science Division, CSIR-Central Electrochemical Research Institute, Karaikudi 630006, Tamilnadu, India

Keywords Nanocomposites · Photoluminescence · Electrochemical · Photocatalytic activity · Thermal analysis

Introduction

In the past 2 decades, nanostructured semiconductors with various structures and morphologies have received much attention due to their novel applications, intriguing properties, and quantum size effects (Cui and Lieber 2001; Xie et al. 2012; Harrison et al. 1999). It is well known that ZnS is a commercially important II–VI group semiconductor having a wide optical band gap, rendering it as a very attractive material for optical application especially in nanocrystalline form. As an intrinsic semiconductor compound, silver sulfide (Ag_2S) possesses a narrow band gap and good chemical stability. In the past few years, Ag_2S nanoparticles have attracted much attention due to their potential applications in photoconductors, solar cells, near-infrared photo-detectors (Xiaodong et al. 2008), and so on. The low-temperature phase of bulk silver sulfide is stable up to approximately 177 °C and is usually denoted as α-Ag_2S. It is well known that α-Ag_2S is a semiconductor with a monoclinic structure (Sadanaga and Sueno 1967) and a band gap of approximately 1 eV at room temperature (Junod et al. 1977).

Recently, attempts have been made to prepare core–shell nanocomposites of both organic and inorganic materials (Murugadoss 2012a, b, 2013). Core–shell nanoparticles often exhibit improved physical and chemical properties over their single-component counterparts, and hence are potentially useful in a broad range of applications. To realize the practical applications of the nanocomposites, it is desirable to develop novel, simple,

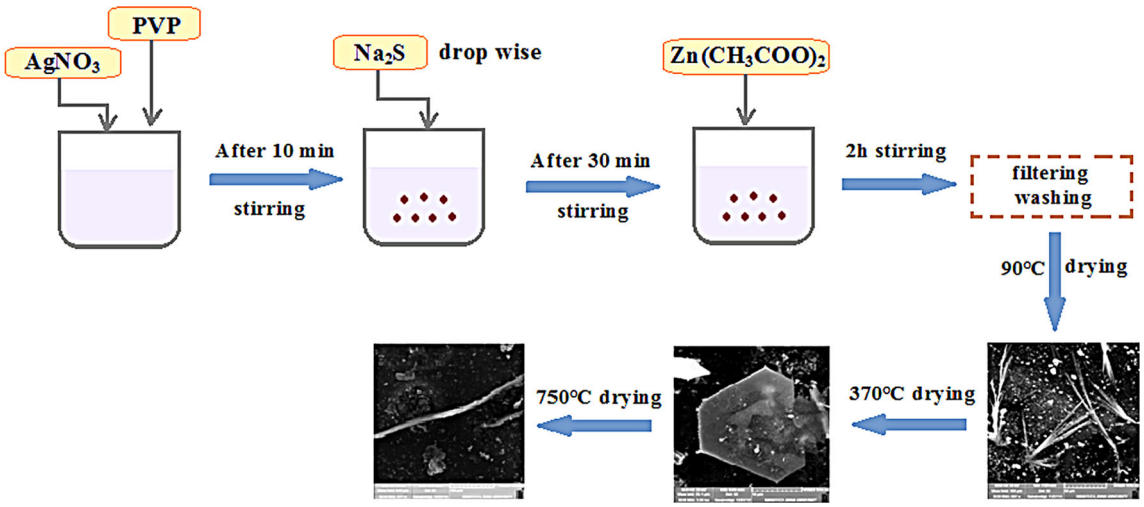

Fig. 1 Schematic of the synthesis of the Ag_2S/ZnS nanocomposites

fast, and low-cost methods for the synthesis of these nanocomposites. The control over nanoparticle size, size distribution, and dispersity is very important for the synthesis of high-performance nanocomposites. Different combinations of metal oxides and metal sulfide have been extensively examined as potential photocatalysts for the degradation of organic dyes (Reddy et al. 2007; Wu and Chern 2006). Heterogeneous photocatalysis is a good method for the decontamination and mineralization of organic pollutants because of its high efficiency, low-energy consumption, and satisfactory environmental compatibility (Su et al. 2008; Žukauskas et al. 2010). In view of this, ZnS and Ag_2S with band gap energy of 3.6 and 0.9 eV, respectively, are considered to be good photo-responsive catalysts. Herein, we have synthesized ZnS/Ag_2S and Ag_2S/ZnS nanocomposites with different morphology such as seeding, spherical, antenna, and rod-like structure by with and without thermal treatment and studied their optical, electrochemical, photocatalytic, and thermal properties.

Materials and method

All chemicals were analytical grade and used as received without further purification. In the whole synthesize process, de-ionized water was used as a solvent. The schematic diagram of the synthesis process is shown in Fig. 1. In a typical synthesis of Ag_2S/ZnS nanocomposites, 50 ml of 0.1 M of sodium sulfide ($Na_2S.xH_2O$) solution was added into 100 ml of 0.1 M silver nitrate ($AgNO_3$) solution, which was stirred vigorously at room temperature. After 30-min stirring, 0.5 M of 50 ml zinc

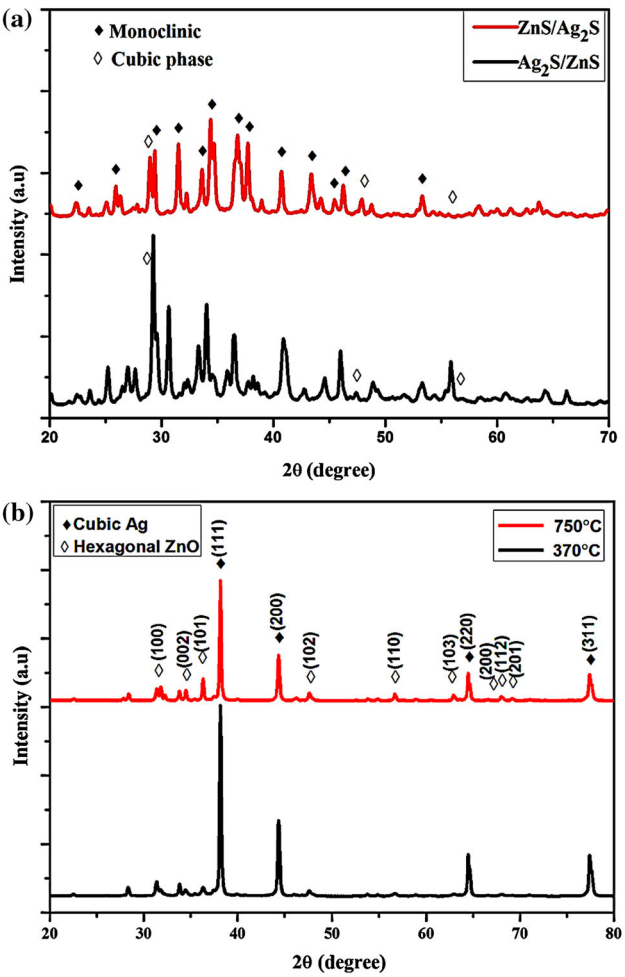

Fig. 2 X-ray diffraction pattern of **a** as-prepared ZnS/Ag_2S and Ag_2S/ZnS nanocomposites; **b** Ag_2S/ZnS nanocomposite annealed at 370 and 750 °C

acetate (Zn $(CH_3COO)_2.H_2O$) was added drop-by-drop into the above colloidal solution, which was stirred for 2 h. Then, the collected precipitate was washed with ethanol and acetone for several times to remove the residual component then dried in hot air oven at 120 °C for 2 h. For synthesize of ZnS/Ag_2S nanocomposites, the above experimental processes was applied in the reverse order.

Characterization

The obtained products were characterized by XRD (Rigaku miniFlex IIC diffractometer), SEM (VEGA 3 SEM), UV–visible absorption (1650PC SHIMADZU spectrometer), and photoluminescence (RF-5301PC spectrophotometer) spectra. Thermogravimetric and differential thermal analyses (TG–DTA) were performed using SDT Q600 20.

Photocatalytic properties study

The photocatalytic activities of the Ag_2S/ZnS and ZnS/Ag_2S nanocomposites were evaluated by degrading methylene blue (MB) in aqueous solution under visible irradiation. Before the reaction, 10 mg photocatalyst was added into 50 mL MB solution (0.01 g/L), and stirred in the dark for 2 h. Then the system was irradiated for 6 h with a 300 W visible lamp with wavelengths of 400–700 nm. Initially, every 5 min, 5 mL solution was taken out of the system and centrifuged at 5000 rpm for 5 min, and the concentration of MB in

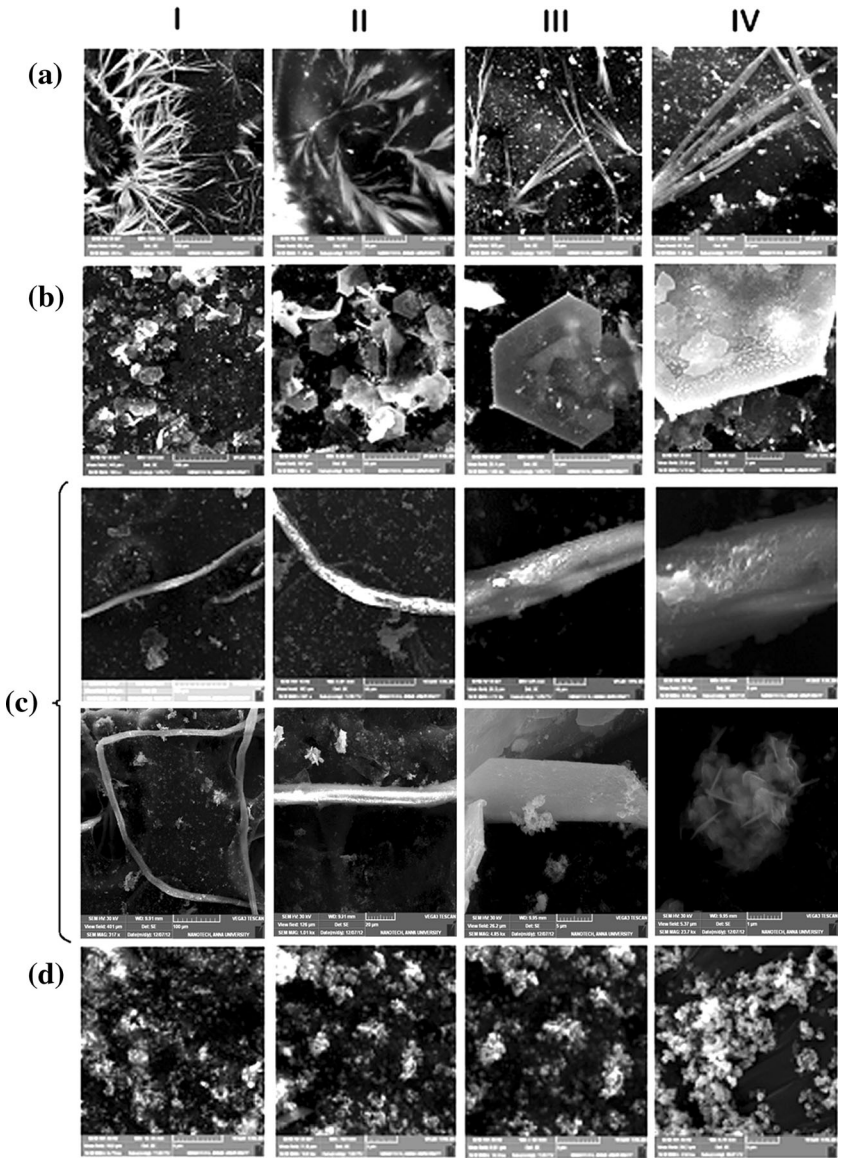

Fig. 3 SEM images of **a** as-prepared Ag_2S/ZnS nanocomposite; **b** Ag_2S/ZnS nanocomposite annealed at 370 °C; **c** Ag_2S/ZnS nanocomposite annealed at 750 °C [for clear evidence, more (8 images) SEM images included]; **d** as-prepared ZnS/Ag_2S nanocomposite

the supernatants was determined with UV–vis absorption spectroscopy.

Electrochemical study

Electrochemical measurements were performed using CHI 660D Biologic electrochemical workstation. In a typical electrochemical measurement, three-electrode cell system composed of Ag_2S/ZnS and ZnS/Ag_2S nanocomposites electrode as the working electrode, a platinum wire as the counter electrode, and an Ag/AgCl as the reference electrode were used. The working electrodes were prepared by coating a slurry containing a mixture of the active material (80 wt %), Nafion®117 solution (20 wt %). The coated mesh was dried at 80 °C in vacuum cabinet overnight. The cyclic voltammetry measurements of the nanocomposites were carried out at a scan rate of 10 mVs^{-1}.

Results and discussion

Structure and crystallinity of the synthesized nanocomposites were confirmed by X-ray diffraction pattern. Figure 2a shows combined X-ray pattern of the Ag_2S/ZnS and ZnS/Ag_2S nanocomposites. As seen in the Fig. 2a, the diffraction peaks of the both samples are broad. It dictates that the particles size is to be in the nanoscale regime. The diffractive peaks marked with the symbol (◆) can be assigned to the monoclinic Ag_2S (JCPDS Card No. 14–0072) and those marked with asterisks (◇) can be assigned to cubic phase of ZnS (JCPDS Card No. 05–0566). The XRD result revealed successful formation of the mixed structured Ag_2S/ZnS and ZnS/Ag_2S nanocomposites by the simple chemical method. The particles size can be estimated by considering the full width half maximum (FWHM) of the XRD peaks using Debye–Scherrer formula. The measured particle sizes are 5.8 and 6.2 nm for Ag_2S/ZnS and ZnS/Ag_2S nanocomposites, respectively. Comparing the XRD patterns (Fig. 2a) of the two nanocomposites, the corresponding diffraction of first compound in the nanocomposites was more dominated than the second one. The fraction of the Ag_2S and ZnS was measured by the most intensity of the diffraction peaks. For Ag_2S/ZnS, the quantitative of Ag_2S is 54.5 % and ZnS is 45.5 %, and 51.2 % (Ag_2S) and 48.8 % for ZnS/Ag_2S. The results show the fraction of Ag_2S is significantly increased than ZnS in Ag_2S/ZnS nanocomposites. This observation can

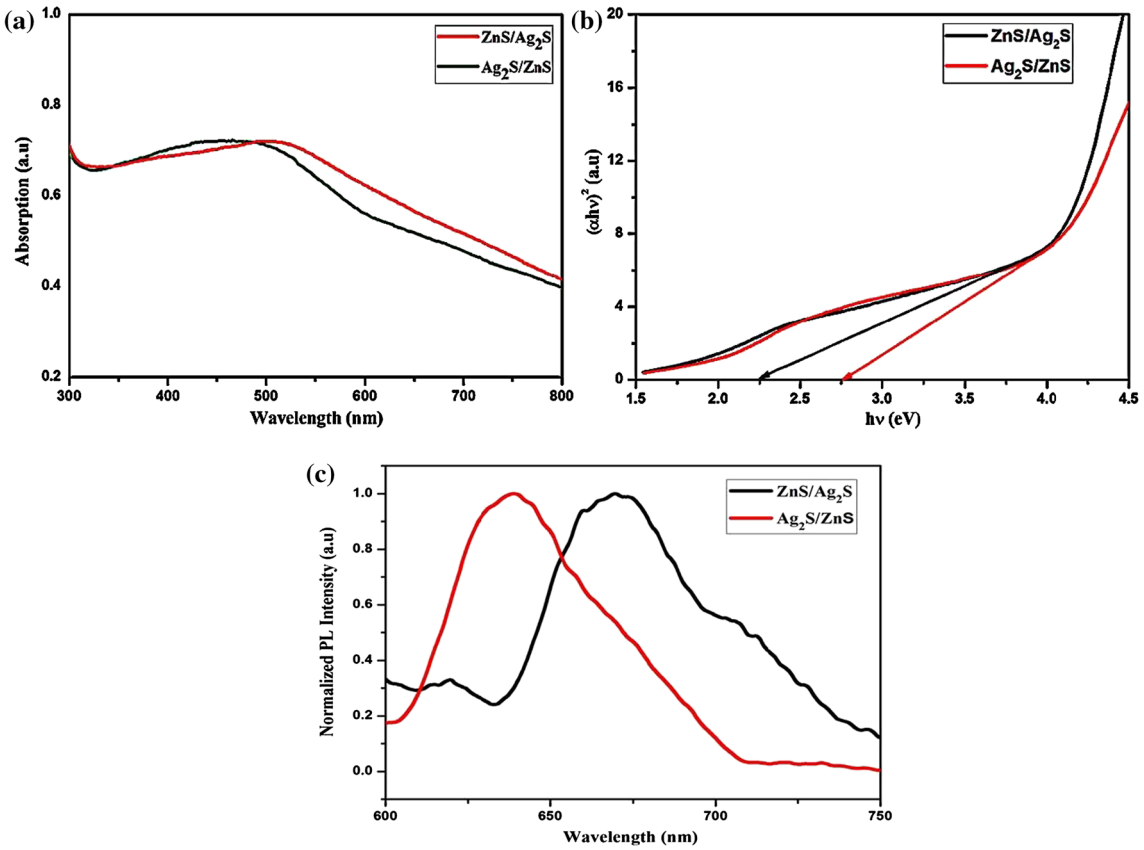

Fig. 4 **a** UV–visible; **b** Tauc plot and **c** PL spectra of as-prepared ZnS/Ag_2S and Ag_2S/ZnS nanocomposites

be explained from the fact that Ag_2S has lesser solubility product constant (K_{sp}; K_{sp} of $Ag_2S = 6 \times 10^{-51}$) than that of ZnS ($K_{sp}$ of $ZnS = 2 \times 10^{-25}$). Because of this, large amount of sulfur ions may consumed rapidly by silver than zinc ions during the course of reactions. Thus, predominant Ag_2S diffraction peaks were observed for both composites.

Figure 2b shows XRD patterns of the Ag_2S/ZnS nanocomposite annealed at 370 and 750 °C for 4 h in air. As shown in Fig. 2b, four strong diffraction peaks are observed for both the annealed samples, assigned to cubic Ag (JCPDS Card No. 87–0717). Among the strong diffraction peaks, hexagonal ZnO (JCPDS Card No. 80–0075) planes are detected with low intensity. It revealed a possibility of the formation of Ag–ZnO nanocomposites from Ag_2S/ZnS nanocomposites under thermal treatment in air. Further, when increasing the annealing temperature from 370 to 750 °C, the average size of the product increased from 16.4 to 34.5 nm. In addition, the diffraction peaks correspond to ZnO was noticeably increased as shown in Fig. 2b. Formation of stable hexagonal ZnO may be due to oxidation of the ZnS by air. But, the XRD pattern (Fig. 2b) of annealed Ag_2S shows that oxidation of Ag_2S to Ag_2O is not favored at higher temperature due to the absence of Ag_2O planes. The diffraction peaks at $2\theta = 38$, 44, and 64° (marked by ◆ asterisks) associated with the face-centered cubic (FCC) phase of metallic Ag (JCPDS No. 04–0783). It clearly indicates the formation of crystalline silver cluster in the ZnO nanoparticles. When annealing above 200 °C, the silver sulfide decomposes and only elemental silver is stable, and the remaining sulfur ions may be released as the form of SO_2 gas (Murugadoss 2011). The secondary products ZnO–Ag may be formed in air as given by the following equations:

$$2ZnS_{(s)} + 3O_{2(g)} = 2ZnO_{(s)} + 2SO_{2(g)} \quad (1)$$

$$Ag_2S + O_{2(g)} = 2Ag + SO_{2(g)}. \quad (2)$$

Figure 3a–d shows SEM micrographs of as-prepared and annealed nanocomposites with different magnifications. Figure 3a (i–iv) shows an interesting surface morphology for the as-prepared Ag_2S/ZnS nanocomposites. These SEM images of the Ag_2S/ZnS nanocomposites are immediately remembered a plant of paddy-like structure. To the best of our knowledge, this is the first investigation on the above morphology for Ag_2S/ZnS nanocomposites. In addition, Ag_2S/ZnS nanocomposites were treated at different temperatures and obtained different morphology as shown in Fig. 3b, c. Figure 3b (i–iv) shows as antenna (*lpda*-shark fin style) shape of Ag_2S/ZnS nanocomposites annealed at 370 °C. Further increasing the temperature to 750 °C, the antenna structure was converted into rod-like shape as shown in the Fig. 3c. For clear evidence, more images (8 images) with different magnifications are presented in Fig. 3c, whereas spherical-shaped smooth surface morphology was obtained for as-synthesized ZnS/Ag_2S nanocomposites as shown in Fig. 3d (i–iv).

UV–visible absorption spectra of Ag_2S/ZnS and ZnS/Ag_2S nanocomposites have been shown in Fig. 4a. A maximum peak position of the nanocomposites is centered at 480 and 520 nm for Ag_2S/ZnS and ZnS/Ag_2S, respectively. The optical band gap of the nanostructures was estimated from the Tauc plot (Tauc and Menth 1972) and presented in Fig. 4b. From the absorption values, the calculated band gap is 2.25 eV for ZnS/Ag_2S and 2.55 eV for Ag_2S/ZnS nanocomposites. The measured band values of nanocomposites are noticeably shifted from the bulk band gap of the corresponding ideal compounds. The band gap value of the bulk Ag_2S and ZnS is 0.9 and 3.6 eV, respectively. Figure 4c depicts photoluminescence spectra of the Ag_2S/ZnS and ZnS/Ag_2S nanocomposites. It is clear from this figure that PL

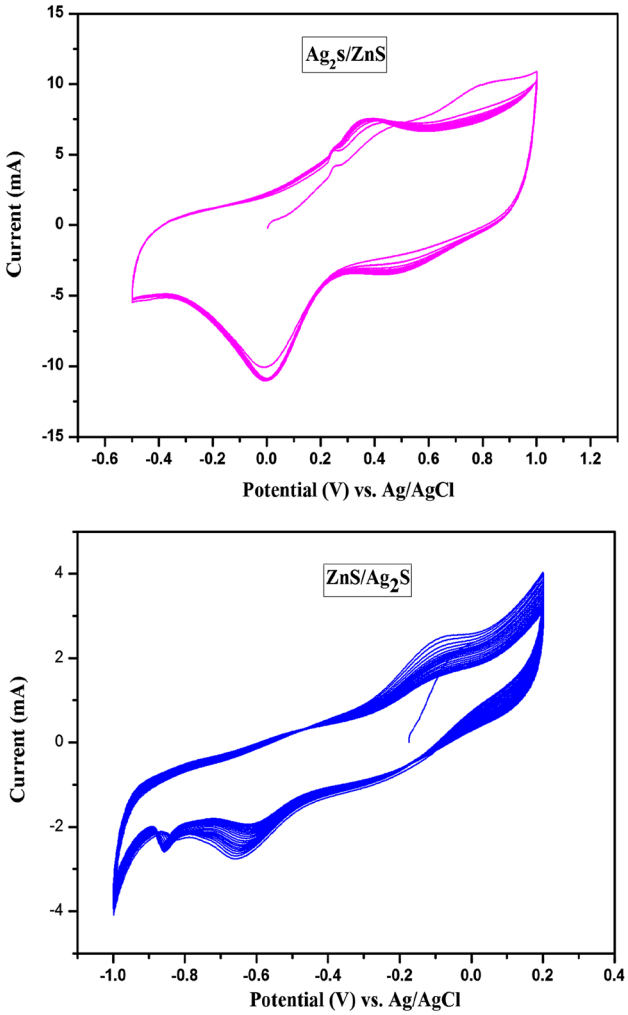

Fig. 5 Cyclic voltammograms of the as-prepared ZnS/Ag_2S and Ag_2S/ZnS nanocomposites. Scan rates = 10 mVs^{-1}

spectra of Ag_2S/ZnS and ZnS/Ag_2S nanocomposites exhibited strong emission in the red region.

When ZnS nanoparticles are coated on Ag_2S and likewise reversely, the blue emission at 450 nm from ZnS and the IR emission about 700–1200 nm range from Ag_2S are absent in both Ag_2S/ZnS and ZnS/Ag_2S nanocomposites. This suggests successful formation of the nanocomposites. For core shell like nanocomposites, the core materials play an important role for tuning the optical emission. The PL spectrum of ZnS/Ag_2S shows a significant red shifting from Ag_2S/ZnS. The red shifting of PL emission for ZnS/Ag_2S may be due to emission of photons from the wide band gap of ZnS and absorption by narrow band gap of Ag_2S, and then recombination process on ZnS/Ag_2S occurs. This results in red emission observed at 670 nm. In addition, this PL emission shows strong blue shifting compared with ideal emission of Ag_2S (Yang et al. 2013). It also revealed a successful formation of ZnS/Ag_2S nanocomposites. To the best of our knowledge, this is the first observation of PL emission at 670 nm for Ag_2S/ZnS nanocomposites. Cyclic voltammetric responses of as-prepared ZnS/Ag_2S and Ag_2S/ZnS samples in acetonitrile with 0.1 M $LiClO_4$ supporting electrolyte are shown in Fig. 5. Ag_2S/ZnS shows well-defined voltammetric response, while ill-defined responses were obtained for ZnS/Ag_2S sample. The shoulder peaks with main redox peaks which may be the presence of some unreacted Ag_2S particles with ZnS/Ag_2S composites.

Photocatalytic behavior of the ZnS/Ag_2S and Ag_2S/ZnS nanocomposites toward degradation of MB under visible light irradiation was investigated and shown in Fig. 6a–c. No detectable degradation of MB was observed without any catalyst under illumination of UV light, which reveals that the degradation occurred was due to catalysts (not shown). The profiles for degradation of MB in the presence of nanocatalysts are shown in Fig. 6c. It can be seen that ZnS/Ag_2S nanocatalysts have higher degradation efficiency than Ag_2S/ZnS nanocomposites. The ZnS/Ag_2S nanocatalysts provide multiple benefits like a dispersing agent and sufficient band gap alignment, which enhances the photocatalytic activity. Furthermore, the higher photocatalytic activities of the ZnS/Ag_2S may be attributed to the separation of electron–hole pairs rather than the transport of charge carriers. On the other hand, lower photocatalytic performance of Ag_2S/ZnS heterostructures may be due to the unfavorable electron transfer and the rapid recombination of electron–hole pairs.

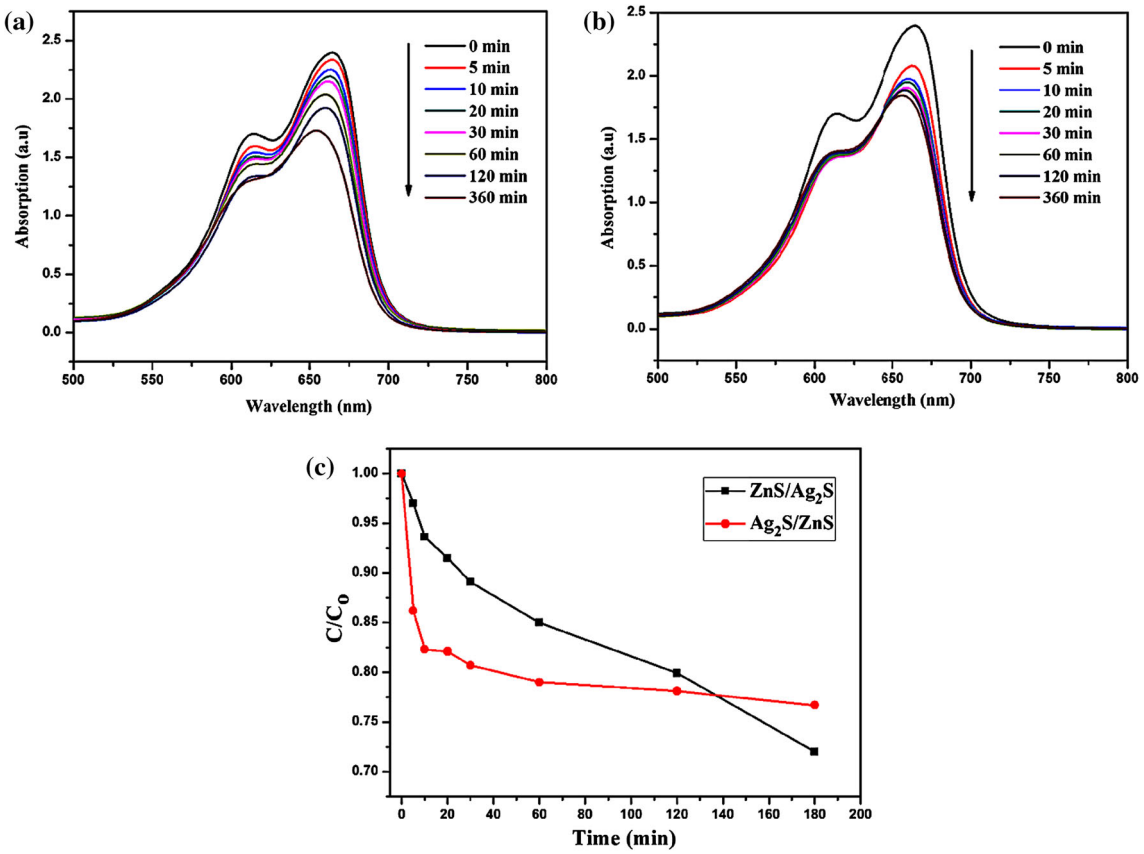

Fig. 6 **a, b** Absorption spectra of the degradation of MB under visible light in aqueous solution and **c** Photocatalytic activity of the corresponding samples (as-prepared)

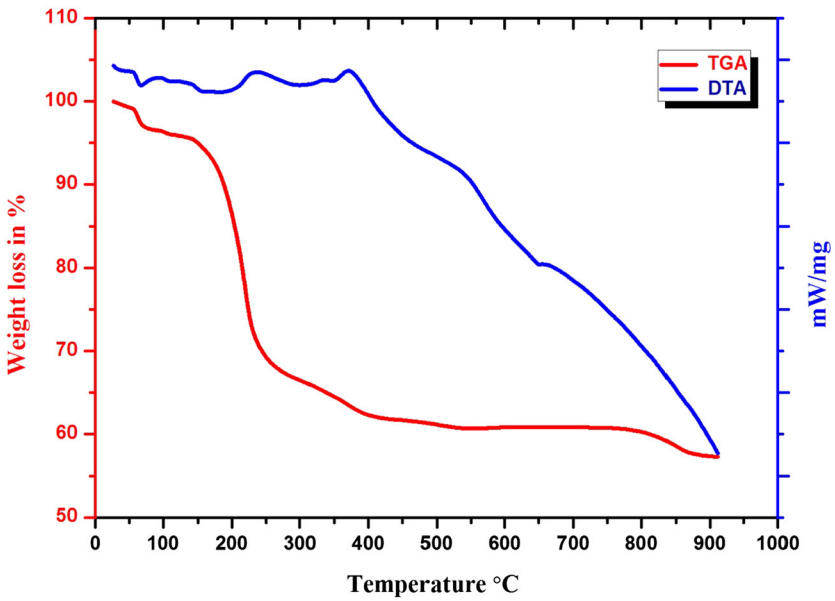

Fig. 7 TG–DTA analyses of as-prepared Ag_2S/ZnS nanocomposite

Figure 7 shows combined TG–DTA plot of Ag_2S/ZnS nanocomposites. As shown in the figure, a minor weight loss is observed below 150 °C. It can be assigned to the loss of adsorbed water on the surface of the nanocomposites. Significant weight loss was shown between 150 and 250 °C in TG curve with corresponding changes in DTA. It can be attributed to the removal of residual compounds and decomposition of major sulfur ions from Ag_2S due to low stability at higher temperature (Frueh 1958). It is in good agreement with XRD result (Fig. 2b). A sharp exothermic peak is observed in DTA curve at 370 °C with corresponding weight loss appears in TG curve from 250 to 550 °C. It may be due to the release of the remaining sulfur ions from core ZnS. Finally, an exothermic peak is observed in the downward curve of DTA curve between 650 and 750 °C with small weight gain in TG curve instead of weight loss at higher temperature. It may be due to conversion of ZnS to ZnO in air as discussed in Fig. 2b.

Conclusion

Here, we have presented the first comprehensive investigation on growth kinetics, optical, photocatalytic, and thermal properties of water soluble Ag_2S/ZnS and ZnS/Ag_2S nanostructures. The XRD measurements indicate the formation of nanocomposites with mixed phases. SEM images of nanocomposites signify the possibility of preparing different morphology Ag_2S/ZnS. The photocatalytic results showed that the binary hybrid, ZnS/Ag_2S nanostructures exhibited an enhanced performance under visible light. First time, high crystal quality of Ag–ZnO nanocomposites was prepared thermally from Ag_2S/ZnS nanocomposite and the possible mechanism was also presented. The strong visible light absorption and fast photocatalytic properties of the nanocomposites promise that they may be used as a sensitizer to fabricate an efficient solar cell, energy storage, and photocatalytic applications.

Acknowledgments The authors would like to thank the Department of Science and Technology, India for the financial support of this work through Nanomission Research Programme (DST–NST, Project No. JNC/AO/A-0610/(16)/12).

References

Cui Y, Lieber CM (2001) Functional nanoscale electronic devices assembled using silicon nanowire building blocks. Science 291:851–853

Frueh AJ (1958) The Crystallography of silver sulfide, Ag_2S, Jr. Z. Kristallogr., Kristallgeom., Kristallphys. Kristallchem 110:136–144

Harrison MT, Kershaw SV, Burt MG, Rogach AL, Eychmuller A, Weller H (1999) Investigation of factors affecting the photoluminescence of colloidally-prepared HgTe nanocrystals. J Mater Chem 9:2721–2722

Junod P, Hediger H, Kilchör B, Wullschleger J (1977) Metal-non-Metal Transition in Silver Chalcogenides. Phil Mag 36:941–958

Murugadoss G (2011) Synthesis, optical, structural and thermal characterization of Mn^{2+} doped ZnS nanoparticles using reverse micelle method. J Lumin 131:2216–2223

Murugadoss G (2012a) Luminescence properties of multilayer coated single structure ZnS/CdS/ZnS nanocomposites. Spectrochimica Acta Part A 93:53–57

Murugadoss G (2012b) Structural and optical properties of monodispersed ZnS/CdS/ZnO and ZnO/ZnS/CdS nanoparticles. J Lumin 132:2665–2669

Murugadoss G (2013) Synthesis and photoluminescence properties of zinc sulfide nanoparticles doped with copper using effective surfactants. Particuology 11:566–573

Reddy MP, Venugopal A, Subrahmanyam M (2007) Hydroxyapatite photocatalytic degradation of calmagite (an azo dye) in aqueous suspension. Appl Catal B 69:164–170

Sadanaga R, Sueno S (1967) X-ray study on the α–β transition of Ag_2S. Mineral J 5:124–143 **Japan**

Su W, Chen J, Wu L, Wang X, Wang X, Fu X (2008) Visible light photocatalysis on praseodymium(III)-nitrate-modified TiO_2 prepared by an ultrasound method. Appl Catal B 77:264–271

Tauc J, Menth A (1972) States in the gap. J Non-Cryst Solids 8:569–585

Wu CH, Chern JM (2006) Kinetics of Photocatalytic Decomposition of Methylene Blue. Ind Eng Chem Res 45:6450–6457

Xiaodong Z, Huaqiang S, Daming H, Shumin J, Xun F, Kui J (2008) Room temperature synthesis and electrochemical application of imidazoline surfactant-modified Ag_2S nanocrystals. Mater Lett 62:2407–2410

Xie Y, Yoo SH, Chen C, Cho SO (2012) Ag_2S quantum dots-sensitized TiO_2 nanotube array photoelectrodes. Mater Sci Eng B 177:106–111

Yang H-Y, Zhao Y-W, Zhang Z-Y, Xiong H-M, Yu S-N (2013) One-pot synthesis of water-dispersible Ag_2S quantum dots with bright fluorescent emission in the second near-infrared window. Nanotechnology 24:055706

Žukauskas A, Vaicekauskas R, Shur MS (2010) Colour-rendition properties of solid-state lamps. J Phys D Appl Phys 43:35406